

Design, Fabrication and Control of a Multi-Material–Multi-Actuator Soft Robot Inspired by Burrowing Worms

Ariel A. Calderón, Joakin C. Ugalde, Juan Cristóbal Zagal, and Néstor O. Pérez-Arancibia

Abstract—We present the design, fabrication and feedback control of an earthworm-inspired multi-material multi-actuator soft robot capable of locomoting inside pipes. The bodies of natural earthworms are composed of repeated deformable structural units, called metameres, that generate the peristaltic body motions required for limbless underground burrowing and above-ground crawling. In an earthworm, each individual metamere is actuated by circular and longitudinal muscles that are activated synchronously by the animal’s nervous system. Here, adopting the basic functional principles of metameric worms, we propose a new pneumatically-driven soft robotic system that mimics the motions and replicates the functionality of a single burrowing earthworm’s segment. The suitability of the proposed approach is demonstrated experimentally through three basic locomotion tests: horizontal motion, vertical motion and oblique motion inside a varying-slope transparent pipe.

I. INTRODUCTION

Earthworms are invertebrates that exhibit an ample diversity of motor behaviors and navigation skills. Most species of this type spend a significant amount of their lives underground, feeding on bacteria and algae, while traveling immersed in moist soils that they dig and burrow through. Earthworms also move above ground, where they reproduce and feed on green plants, displaying amazing locomotion capabilities as they maneuver inside intricate cavities, pass through narrow passages and climb inclined and vertical rough surfaces. Instead of limbs, these animals employ hydrostatic structures and muscles (radial and longitudinal) to deform, stretch and adapt volumetrically while transmitting forces to the environment. Specifically, earthworms move by generating retrograde peristaltic waves that pass through their bodies, produced by the expansion (relaxation) and contraction of longitudinal and segmented circular muscles, thus inducing synchronized axial and radial deformations of their body segments [1]–[5]. This kind of locomotion enables worms to move stably and efficiently in highly unstructured environments, such as burrows, irregular terrains, trees and convoluted pathways [1], [6].

In this work, we replicate some of the earthworms’ mechanisms of motion by developing new actuation and sensing methods based on multi-material soft robotic technology. The synthesis of artificial systems able to replicate the capabilities of earthworms represent a significant step forward in the development of autonomous robots, medical robots and soft

mechatronic systems in general. Numerous attempts aiming to replicate the locomotion mechanisms of metameric worms have been published in the technical literature [7], which describe the application of a wide variety of technologies to the problem, including *shape memory alloys* (SMAs) [5], [8], [9], magnetic fluids [10], electric motors [6], [11], [12] and even simple versions of semi-soft actuators [13], [14]. However, to this date, the functional characteristics of natural worm-muscles have not been fully replicated due to technological limitations that only recently have been overcome with the emergence of innovative fabrication methods. This technological progress has enabled the development of novel biologically-inspired soft actuators, soft sensors and flexible electronics [15]–[18]. These emergent technologies are advanced in this work for the development of the proposed robotic concept inspired by earthworms.

A distinguishing characteristic of soft robotic systems is their ability to smoothly function in and adapt to the inhomogeneous time-varying geometrical conditions that they might encounter in the environments in which they operate. Likewise, adaptability is the most noticeable feature of some invertebrates, such as worms and squids, correspondence that makes possible the creation of robots designed upon or inspired by natural systems. For example, [15] describes the design and development of a multi-gait highly-flexible pneumatically-driven soft robot capable of walking on unstructured surfaces and performing other tasks difficult to achieve by rigid robots. In that case, the system’s soft limbs are actuated synchronously by injecting air with different pressure levels into different stretchable chambers fabricated inside the legs, which are pre-programmed by design to deform according to predictable patterns in response to pre-specified open-loop control air pressure inputs. Also, several recent publications [19]–[23] have presented the development of reinforced multi-material bending actuators, some of which have been demonstrated to achieve extremely large curved deformations, even exceeding those observed in the limbs of *soft animals*. Similarly, [24] describes a soft robotic mechanism capable of emulating, to some extent, the movements of a living octopus’ tentacle.

The earthworm-inspired soft robot proposed here is assembled of two types of pneumatically-driven multi-material actuators, axial and radial, that mimic the functions of the longitudinal and circular muscles found in earthworms (see Fig. 1). The basic conceptual robotic design and fabrication methods introduced in the development of the proposed worm-inspired robot are the main contributions of this work. These outcomes have been achieved by relying mainly on rapid prototyping techniques based on the use of 3D-printed molds, curable liquid silicone and soft lithography [25]–[27].

Here, as always, the problems of robotic development, fabrication and control are strongly coupled, as the way materials are integrated together to create the mechanically pre-programmable robot’s actuators determines the pre-

Preliminary results of this work were presented in a poster at the 2016 Southern California Robotics Symposium (SCR 2016).

This work was supported in part by the Chilean National Office of Scientific and Technological Research (CONICYT) through a graduate fellowship to A. A. Calderón, and in part by the USC Viterbi School of Engineering through a graduate fellowship to A. A. Calderón and a start-up fund to N. O. Pérez-Arancibia.

A. A. Calderón and N. O. Pérez-Arancibia are with the Department of Aerospace and Mechanical Engineering, University of Southern California (USC), Los Angeles, CA 90089-1453, USA (e-mail: aacalder@usc.edu; perezara@usc.edu). J. C. Ugalde and J. C. Zagal are with the Department of Mechanical Engineering, FCFM, University of Chile, Santiago, 8370448, Chile (e-mail: joakin.ugalde@ing.uchile.cl; jczagal@ing.uchile.cl).

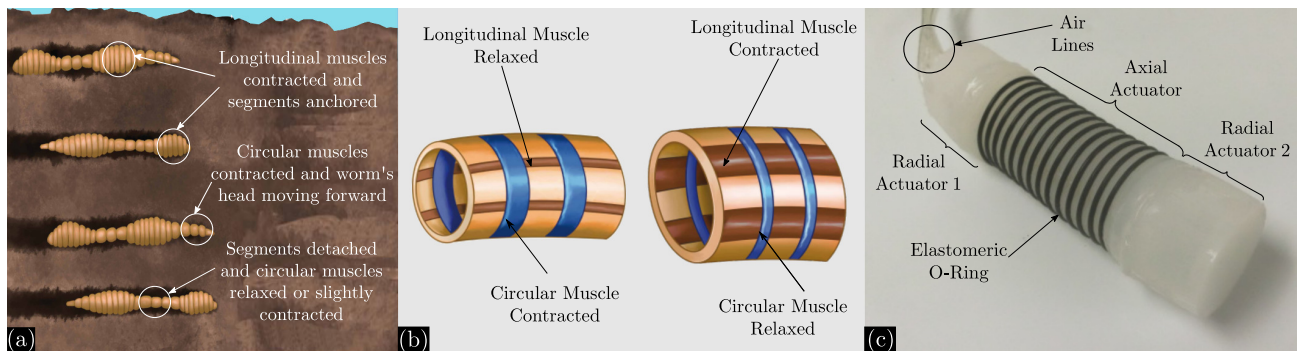


Fig. 1: **Natural and artificial worms.** (a) Illustration showing the peristalsis-based locomotion of earthworms during burrowing. (b) Illustration showing a segment of an earthworm's body. The *blue* rings represent circular muscles that contract and relax radially and the *brown* stripes represent longitudinal muscles that contract and relax linearly, both required to generate body peristaltic waves. (c) Picture showing the biologically-inspired soft robot presented in this paper. The robot is composed of three actuators: a rear radial actuator, a central axial actuator and a frontal radial actuator. The two radial actuators are the artificial analogues of the circular muscles in *blue* in Fig. 1-(b) and the axial actuator is the artificial analogue of the longitudinal muscles in *brown* in Fig. 1-(b).

programmable dynamics of the resulting system. Therefore, from a holistic perspective, the controllability properties of the soft robot are pre-determined (pre-programmed) at the time of fabrication. In this case, the dynamic responses (deformations) of the actuators generated during operation are pre-programmed with the use of structural fibers and elastomeric circular rings (o-rings) that reinforce and constrain the deformations of the soft materials composing the actuators when air is injected to them. In this way, the time-varying shapes that the soft robot takes and the forces it exerts on the environment can be chosen and varied in real time with the use of air-pressure-based feedback control.

Further extensions of the ideas and results presented in this paper can be applied to the creation of wide variety of mechatronic systems, including autonomous robots for internal pipe inspection, millimeter-scale robotic assistive tools for cardiac and digestive surgeries (advanced extensions of the notions and results in [11], [12], [23], [28], for example) and even microrobots capable of navigating inside the human body circulatory and digestive systems in order to perform micro-surgical or pharmacological tasks (as imagined by some science fiction writers [29]), just to mention a few number of possibilities.

The rest of the paper is organized as follows. Section II describes some basic notions of biologically-inspired locomotion in robotics, Section III explains the design, fabrication and characterization processes employed in the creation of the actuators composing the proposed earthworm-inspired soft robot. Section IV discusses locomotion planning and associated control strategies. Experimental results are shown and discussed in Section V, and lastly, conclusions are drawn in Section VI.

II. BIOLOGICALLY INSPIRED LOCOMOTION

The study of locomotion is essential for the development of autonomous robots capable of operating in real-life scenarios with time-varying conditions and information-rich terrains. Significant progress on wheeled and multi-pedal locomotion for autonomous robotic applications has been reported during the last decade [30]–[33]. Similarly, the locomotion modes of legless animals have served as inspiration in the development of artificial snakes [34]–[36], using hard and soft robotic technologies. In many cases, snake-inspired limbless crawling is advantageous due to its low complexity and energetically efficient use of friction forces

[34], [35]. Another interesting legless locomotion mode is the one exhibited by earthworms. These animals actively shape their hydrostatic skeletons, integrated with circular and longitudinal muscles, to perform the mechanical actions required for locomotion. Thus, as the earthworms' muscles synchronously extend and contract to produce body peristaltic waves, the earthworms' hydrostatic skeletons directly transmit oscillatory forces to the environment. Hydrostatic skeletons observed in nature are not only deformable but also adaptable as their stiffnesses are dynamically varied, features that can be mimicked by soft robots [1], [2].

Earthworms (*lumbricus terrestris*) belong to the phylum *annelida* (from Latin, *annelus* = little ring + *ida* = plural suffix), characterized by worms whose bodies are composed of ring-shaped segments (metameres) connected in series, as shown in Fig. 1-(a). Annelids evolved bodies in which each metamere contains similar components of all the major organ systems. Because at constant temperatures and pressures the volume of fluids remains essentially constant, in hydrostatic skeletons, contraction of the longitudinal muscles in Fig. 1-(b) causes a body's segment to shorten, whereas contraction of the circular muscles in Fig. 1-(b) causes a body's segment to lengthen and become thinner. Some biologists have argued that the evolution of hydrostatic skeletons composed of separated metameres greatly increased the efficiency of worms' dynamics [1], because the force of local muscle contraction within one segment is not transferred and dampened along the length of the animal. This segmented pattern of muscle action is what enables worms to generate the alternating body waves of contractions and elongations (peristalsis) observed during crawling and burrowing.

Also, earthworms belong to the class *oligochaeta*, characterized by worms whose body segments bear a few number of small bristle-like rods (*setae*), used during crawling and burrowing to anchor parts of the body to the ground or surrounding soil in order to prevent slipping. The specific mechanisms employed during burrowing are graphically described in Fig. 1-(a) and Fig. 1-(b), which is the basic locomotion mode we take as inspiration for the creation of the robot presented in this work. Considering Fig. 1-(a), here we say that a *stride* is the cyclical kinematic process that occurs between two consecutive identical geometrical configurations of the worm-burrow system, or equivalently, one cycle of peristalsis. This is an idealization for the

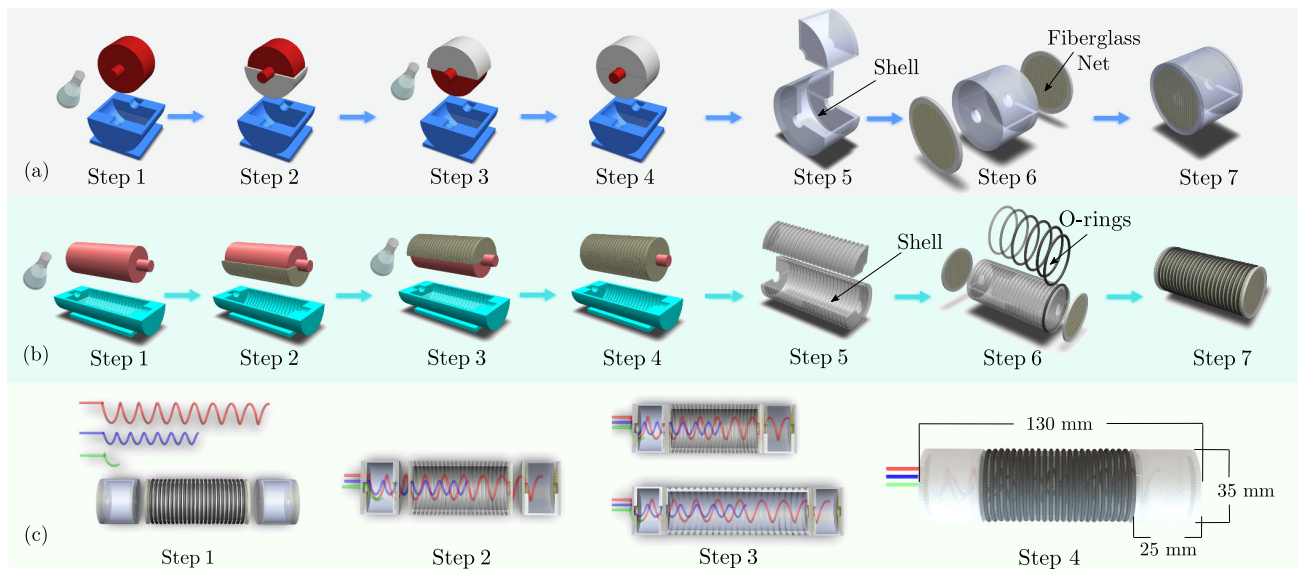


Fig. 2: **Fabrication methods and robot's construction.** The fabrication processes use as physical inputs 3D-printed molds made of *acrylonitrile butadiene styrene* (ABS), silicone elastomer (Ecoflex[®] 00-50, Smooth-On), butadiene rubber elastomeric o-rings, sheets of fiber glass and pneumatic components. The robot's construction consists of three parts ((a), (b) and (c) shown above), each consisting of several steps. **(a) Fabrication of a radial actuator:** First, liquid silicone is poured into a half-cylindrical mold and the lower half of a symmetric plastic cylindrical shaft is submerged in the liquid (Step 1). In Step 2, the mold and silicone are exposed to 60°C for 30 minutes, resulting in a cured half-cylindrical shell that covers half of the shaft. In Steps 3 and 4, the shaft and the attached half-cylindrical shell are rotated 180° and the procedures in Step 1 and Step 2 are then repeated to create the second half of the shell. In Step 5, the shaft is removed to obtain a cured silicone cylindrical shell. In Step 6, the frontal and rear circular faces of the cylindrical shell are sealed and reinforced with sheets of laminar composite made of soft silicone and a fiber glass net. This structural reinforcement is implemented to prevent significant radial deformations of the circular docking faces while preserving the soft nature of the system axially. In this case, the sub-components are glued to each other and sealed by applying external liquid layers of silicone to them. Finally, once the end-caps are cured and sealed, the actuator is completed (Step 7). This process requires the pre-degasification of the liquid silicone in order to prevent the generation of air bubbles that might produce undesired shapes and weak structural points. **(b) Fabrication of an axial actuator:** This process uses the same procedures used in the fabrication of a radial actuator in 7 steps, shown in (a). In this case, the mold contains imprinted grooves to lock up butadiene o-rings in position during Step 6. **(c) Final assembly:** Two radial actuators, an axial actuator and three helix-shaped air feeding lines are integrated into a single functional body. Similar to what is described in Step 6 of (a), the actuators are glued to each other and sealed by applying liquid layers of silicone to them. Notice that the helical shape of the air lines is a critical design feature of the robotic system that allows for the expansion and contraction of the soft actuators.

purposes of analysis, and therefore, two configurations are considered identical if in both of them, exactly the same segments are anchored or detached, without considering other physical variables. This definition is analogous to that of the human case, where a stride equals one complete cycle of a leg, or two steps.

The kinematics of peristalsis-based crawling and burrowing are typically described as a functions of four variables [4]. The first variable is *stride length*, defined as the distance traveled by the first worm's segment during a cycle. The second variable is *protrusion time*, defined as the amount of time in a cycle during which the first worm's segment is moving forward. The third variable is *stance time*, defined as the amount of time in a cycle during which the first worm's segment remains anchored against the ground or burrow. Thus, it follows that the *stride period*, the fourth variable, is simply the sum of the protrusion time and stance time.

The resulting dynamics associated with burrowing-like motion have several advantages over those of other locomotion strategies when designing biologically-inspired robots capable of traveling inside narrow tunnels or pipes. For example, the segmented configuration of earthworms can be translated into mechatronic systems composed of modular identical components (artificial metameres) connected in series, which enables the creation of robots more robust against accidents and component failure. Additionally,

inherent modularity brings an intrinsic capability for reconfigurability and adaptability, which in principle makes possible operation in a wide variety of uncertain environments, employing a multiplicity of locomotion modes. Here, we describe the development of a soft robot, shown in Fig. 1-(c), pneumatically driven by actuators programmable to deform according to configurations similar to those of the muscles in segmented earthworms. This robot can be thought of as an artificial analogue of a single earthworm's metamer, where the animals's morphology is not blindly copied, but employed as inspiration in the replication of some of the relevant functional capabilities of natural earthworms. In this approach, specific parameters of the actuators' dynamics relevant for the creation and implementation of control algorithms are identified through off-line mechanical characterization tests. Thus, the control problem reduces to the generation in real time of the input signals (air pressures) that produce the proper stride lengths, protrusion times and stance times required to effectively mimic the locomotion modes of natural earthworms while burrowing. The specifics are discussed in the next section of this paper.

III. DESIGN, FABRICATION AND CHARACTERIZATION

The soft robot presented in this paper, shown in Fig. 1-(c), is composed of three *artificial muscles*: a back radial actuator, a central axial actuator and a frontal radial actuator. From the biologically-inspired engineering perspective, the robot

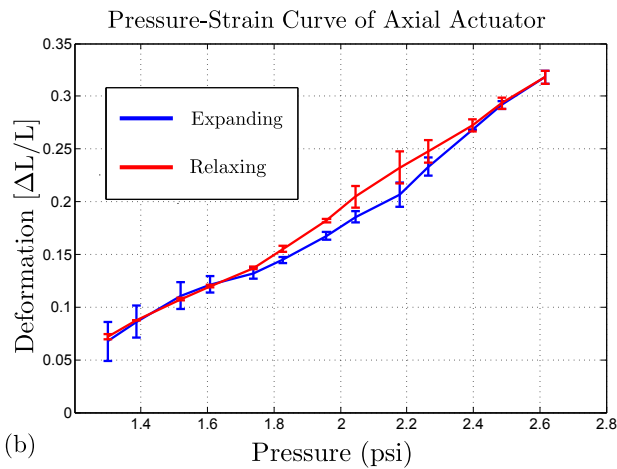
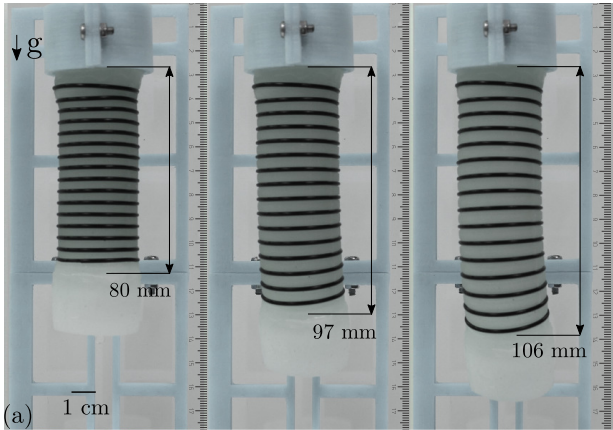


Fig. 3: **Characterization of the axial actuator.** (a) Axial actuator during characterization experiments. (b) Experimental pressure-strain curves associated with the axial actuator. The vertical bars indicate the magnitudes of the *experimental standard deviations* (ESDs). Different from the case of natural muscles, this actuator expands when it is activated and contracts when it is relaxed.

replicates the functional capabilities of an earthworm's body segment (metamere), illustrated between *blue* rings in Fig. 1-(b). The first type of soft actuator, shown in Fig. 1-(c) and Fig. 3-(a), is driven pneumatically and replicates the features of earthworms' longitudinal muscles. This structural configuration allows for linear axial elongations and contractions as functions of the internal air pressure, while preserving, to a significant extent, the radial dimension. The second type of soft actuator, shown in Fig. 1-(c) and Fig. 4-(a), replicates the features of earthworms' circular muscles. This structural configuration allows for radial expansions and contractions as function of the internal air pressure, while preserving, to some extent, the axial dimension.

In the proposed robotic design, the main purpose of the posterior and anterior actuators is to anchor the robot to the surrounding terrain (in this case, the internal surface of a pipe), while the axial central actuator enables the controlled expansions and contractions of the robot during locomotion. Notice that the proposed artificial muscles mimic the mechanical functions of natural muscles, but their underlying working mechanisms are fundamentally different. Natural muscles are incapable of elongating actively and deformation is always produced by active contraction. Therefore, in the natural case, the word relaxation is typically used as a synonym for passive elongation. In contrast, the soft actu-

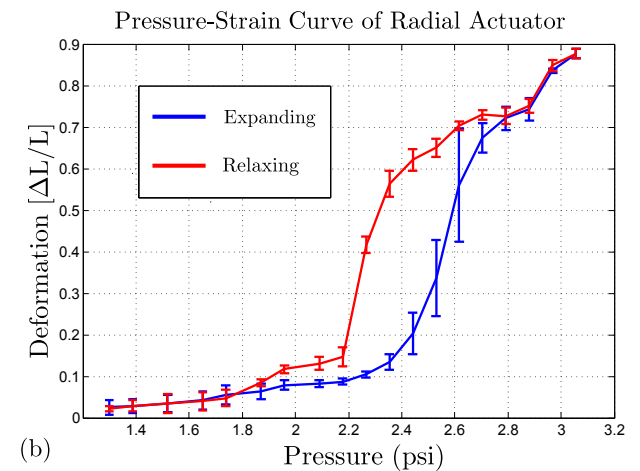
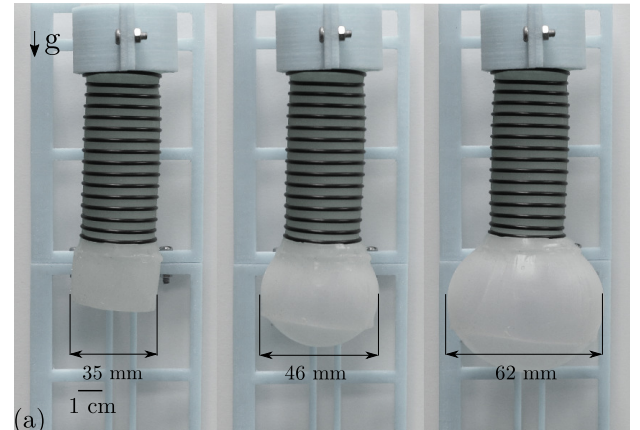


Fig. 4: **Characterization of the radial actuator.** (a) Radial actuator during characterization tests. (b) Experimental pressure-strain curves associated with the radial actuator. The vertical bars indicate the magnitudes of the *experimental standard deviations* (ESDs). Different from the case of natural muscles, this actuator expands when it is activated and contracts when it is relaxed.

ators described here expand actively and contract passively. Consequently, in this particular artificial case, the word relaxation is employed as a synonym for passive contraction.

The fabrication methods and construction sequence used in the manufacture of the soft actuators and final assembly of the robot are graphically described in Fig. 2. Here, Fig. 2-(a) and Fig. 2-(b) illustrate the casting processes employed to fabricate the radial and axial actuators, respectively. In both cases, the fabrication method uses as physical inputs 3D-printed *acrylonitrile butadiene styrene* (ABS) molds, silicone elastomer (Ecoflex[®] 00-50, Smooth-On), butadiene rubber elastomeric o-rings, sheets of fiber glass and pneumatic components. The steps composing the final assembly of the robot are shown in Fig. 2-(c). In this case, the relaxed external roughly-cylindrical dimensions of the resulting soft system are 130 mm in length and 35 mm in diameter, where the wall-thickness of all the components is approximately homogeneous with a value of 2 mm. These dimensions were chosen empirically in order to create a prototype easily testable in laboratory conditions using off-the-shelf transparent pipes.

In open loop, the actions and dynamics of the three robot's actuators are essentially uncoupled, and for this reason, they are characterized individually. An experimental test for the characterization of the axial actuator is shown in

Fig. 3-(a) and the associated resulting pressure-strain curve is shown in Fig. 3-(b). Similarly, an experimental test for the characterization of a radial actuator is shown in Fig. 4-(a) and the associated resulting pressure-deformation curve is shown in Fig. 4-(b). In these experiments, the pressure-strain curves are obtained by measuring a set of static points of pressure and deformation in cycles of increasing plus decreasing pressure. To obtain each data point, the internal actuator pressure is regulated and measured employing a pneumatic assembly composed of a relief solenoid valve (12-V/4-psi generic) in series with a pressure pump (12-V ROB-10398) and a digital serial silicon sensor (Honeywell ASDX), whose output is sent to an Arduino® Mega board used for data acquisition and signal processing. The other entry of each data point (static strain of the tested actuator) is simply measured with a caliper. For each actuator, the measurement cycles are repeated six times.

In the characterization of the axial actuator (Fig. 3), each test cycle is composed of 13 *expanding-direction* static data points and 13 *relaxing-direction* static data points. As can be seen in Fig. 3-(b), the static air pressure is increased in increments of approximately 0.1 psi from 1.3 psi to 2.6 psi, and then, decreased in decrements of 0.1 psi from 2.6 psi to 1.3 psi. In the specific case of Fig. 3, the relaxed length of the actuator is 80 mm, reaching a maximum elongation of 106 mm (an expansion of 33 %) at 2.6 psi. The radial expansion of the axial actuator is not shown, as it is negligible compared to the axial deformation. In Fig. 3, it can be clearly seen that the actuator exhibits a small but non-negligible hysteretic behavior and each strain data point exhibits a significant experimental variance.

In the characterization of the radial actuators (Fig. 4), each test cycle is composed of 19 *expanding-direction* static data points and 19 *relaxing-direction* static data points. As can be seen in Fig. 4-(b), the static air pressure is increased in increments of approximately 0.1 psi from 1.3 psi to 3.1 psi, and then, decreased in decrements of approximately 0.1 psi from 3.1 psi to 1.3 psi. In the specific case of Fig. 4, the relaxed diameter of the actuator is 40 mm, reaching a maximum size of 62 mm (an expansion of 87 %) at 3.1 psi. Unlike the axial actuator, the radial actuator deforms significantly along the axial direction. Also, similar to the case of the axial actuator, in Fig. 4-(b) it can be seen that the radial actuator exhibits a marked hysteretic behavior and each deformation data point exhibits a noticeable experimental variance, facts that indicate the need for the use of feedback control in the implementation of locomotion strategies.

IV. LOCOMOTION PLANNING AND CONTROL

The biologically-inspired actuation sequence employed for locomotion is shown in Fig. 5. Here, five *phases* are defined to generate one *stride* and two possible *conditions* are defined for each actuator as

$$x_{i,k} = \begin{cases} 1 & \text{if } p_i \geq p_{ti} \\ 0 & \text{if } p_i < p_{ti} \end{cases}, \quad (1)$$

where $i = 1, 2, 3$ denotes an actuator according to the convention *rear*, *central* and *frontal*, $k = 1, \dots, 5$ denotes the actuator's phase, p_i is the measured internal pressure of Actuator i and p_{ti} is the threshold pressure to be crossed by Actuator i to change its condition, empirically chosen for controlled extension and contraction. From (1), it follows that the state of Actuator i takes the value 1 when it is

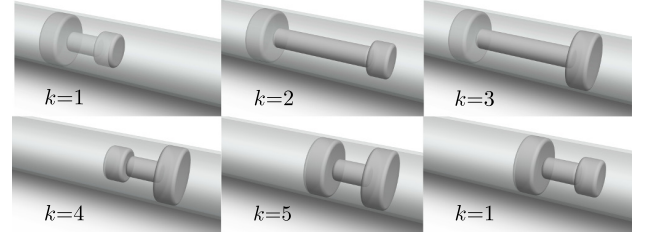


Fig. 5: **Five phases used by the robot to generate one stride.** At $k = 1$, the rear radial actuator is anchored to the pipe. At $k = 2$, the axial actuator is extended reaching a further point. At $k = 3$, the frontal radial actuator is anchored to the pipe. At $k = 4$, the rear radial and axial actuators are relaxed. At $k = 5$, the rear and frontal radial actuators are anchored to the pipe.

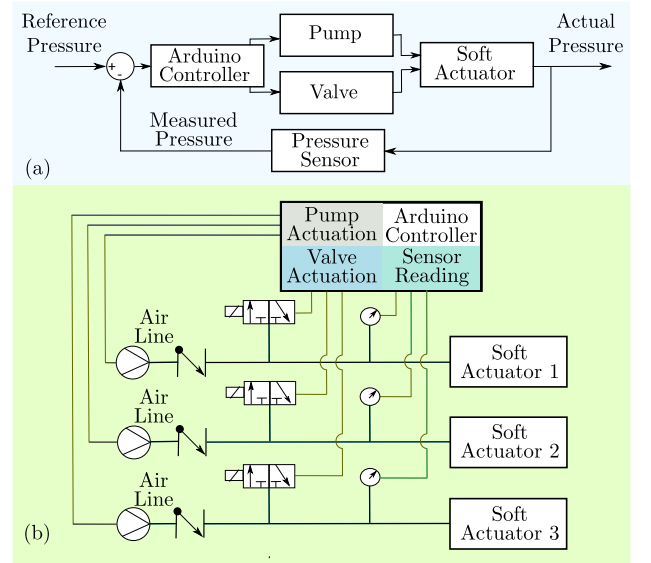


Fig. 6: **Diagrams of the scheme used to control the soft robot during locomotion tests.** (a) Block diagram of the control loop associated with a generic Actuator i . (b) Physical connections of the hardware elements composing the robotic system.

expanded and the value 0 when it is *relaxed*. Notice that this definition of the system's state is completely arbitrary and reflects a binary logical condition of the actuator, used for the design and implementation of the robot's locomotion path. Consequently, the value of the variable $x_{i,k}$ should not be interpreted as an indication that Actuator i is physically totally extended or totally contracted.

The conditions of the three actuators during each phase k of a stride are shown in Table I. For each Actuator i , an air-pump increases the pressure p_i until p_{ti} is surpassed, or a relief valve decreases p_i until its value goes below p_{ti} , triggering the next *stride phase*. The threshold pressures are chosen by employing the experimental information in Fig. 3 and Fig. 4, obtained during the characterization process described in Section III, and are setup to be $p_{t1} = 2.2$ psi, $p_{t2} = 2.4$ psi and $p_{t3} = 2.2$ psi. Notice that as can be seen in Fig. 3-(b) and Fig. 4-(b), the selected pressure thresholds make the robot's actuators relax and expand in agreement with the desired robot's deformations required for locomotion inside pipes. Also, note that for the proposed robot, the axial expansion of Actuator 2 during a cycle is the *stride length*, the time it takes for Actuator 2 to expand

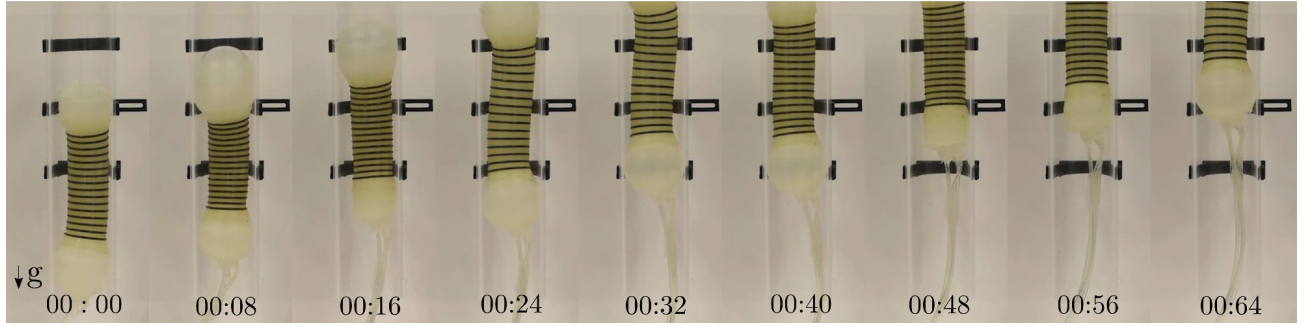


Fig. 7: **Vertical locomotion test.** The robot moves vertically inside a transparent pipe, overcoming gravity as it is able of lifting its own weight. The numbers on the bottoms of the stills show time in minutes:seconds. This experiment was performed at the USC AMSL.

TABLE I: Values of the robot's state, $x_{i,k}$, during each phase k .

Phase k	1	2	3	4	5
Rear Radial Actuator ($i=1$)	1	1	1	0	1
Central Axial Actuator ($i=2$)	0	1	1	0	0
Frontal Radial Actuator ($i=3$)	0	0	1	1	1

during a cycle is the *protrusion time* and the *stance time* is given by the amount of time during a cycle that the frontal actuator remains static (anchoring time + time anchored + detaching time), according to the strategy in Fig. 5. Clearly, these three variables directly depend on the thresholds p_{vi} and the rates of the airflows used to expand the actuators.

The use of the proposed locomotion method requires the implementation of low-level controllers on the individual actuators. The basic control scheme for each actuator is shown in Fig. 6-(a) and the high-level hardware and control scheme of the whole robotic system is shown in Fig. 6-(b). Here, each actuator employs one pump to trigger and sustain actuation. Piezo-resistor-based pressure sensors are employed in the implementation of the low-level control loops in Fig. 6-(a) and high-level control algorithms in Fig. 6-(b). Solenoid valves are used to vary and regulate the pressures inside the actuators. Thus, when a valve is closed, the corresponding actuator's internal pressure increases, as its pump supplies air continuously. Analogously, when a valve is open, the corresponding actuator relaxes and reaches the atmospheric pressure. All the control algorithms in Fig. 6 are run on an Arduino[®] processor.

V. EXPERIMENTAL RESULTS AND DISCUSSION

The final robot prototype and the associated control strategy were tested by performing three locomotion experimental tests, conducted at the USC *Autonomous Microrobotic Systems Laboratory* (AMSL). The first experiment, shown in the photographic sequence of Fig. 7, demonstrates vertical locomotion. This test is relevant because it proves that the robot is dynamically capable of supporting its own weight while following a desired kinematics for locomotion under air-pressure feedback control. The second experiment, shown in the photographic sequence of Fig. 8, demonstrates horizontal locomotion inside a pipe with constant diameter, which is the simplest operating condition that the robot might encounter. The third experiment, shown in the photographic sequence of Fig. 9, demonstrates the ability of the robot to adapt its flexible body in order to maneuver through an uneven path. In this case, the robot begins to move inside a horizontal pipe and then passes through an elbow to continue climbing inside a 45°-inclined pipe section. The complete series of

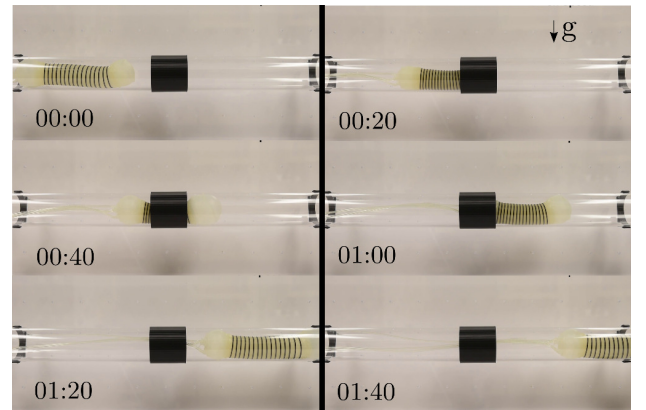


Fig. 8: **Horizontal locomotion test.** The robot simply moves horizontally inside a transparent pipe. The numbers on the lower-left corners of the stills show time in minutes:seconds. This experiment was performed at the USC AMSL.

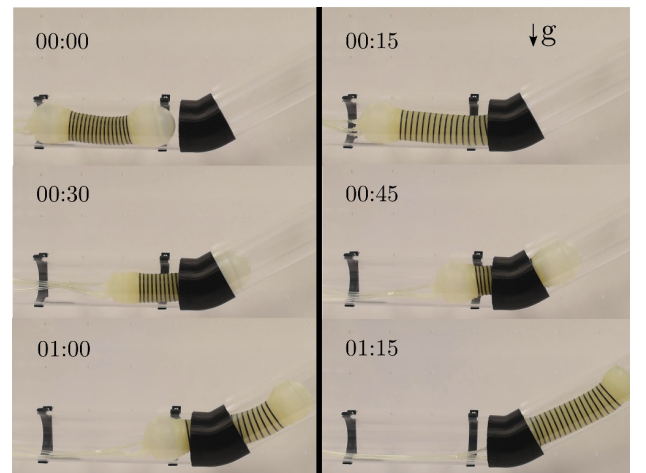


Fig. 9: **Oblique locomotion test.** The robot starts to move horizontally and then adapts its body to maneuver through a path angle of 45°. The numbers on the upper-left corners of the stills show time in minutes:seconds. This experiment was performed at the USC AMSL.

horizontal, vertical and inclined locomotion experiments can be found in the supporting movie S1.mpg, also available at <http://www.uscams1.com/resources/ROBIO/S1.mp4>.

Analysis of the supporting movie S1.mpg shows that the robotic system operates effectively despite occasional sliding during vertical locomotion and unprogrammed/undesired

TABLE II: Measured locomotion parameters during tracking test.

Locomotion Parameter	Value
Stride Length	5.0 cm
Stance Time	5.8 s
Protrusion Time	4.2 s

length changes of the axial actuator when the radial actuators, by pressure variations, are anchoring to or detaching from the internal surface of the pipe. These phenomena represent uncertainty and disturbances that make necessary the use of feedback for locomotion control. As already explained in Section IV, in this work, the measured variable feedback to the controller is internal air-pressure. However, another way to implement feedback controllers is the use of the actual instantaneous kinematics of the robot, which can be measured using external motion capture systems like the one used in [37] or internal flexible strain sensors like those used in [38], which is a matter of further research.

Finally in this section, we discuss the resulting experimental kinematics of a second *twin* robotic prototype (shown in Fig. 10), fabricated and tested at the University of Chile, while locomoting inside a 45°-inclined pipe (as in Fig. 9). In this case, the robot's motion is captured by tracking infrared optical markers attached to both distal non-deformable ends of the robot, employing an OptiTrack® system. Then, from simple calculations, the axial deformation of the robot is obtained. The resulting periodic signal is shown in Fig. 11. The shape of the signal in Fig. 11-(a) indicates that the internal pressure-based feedback strategy is effective for locomotion control, without the need for directly measuring the instantaneous geometry or kinematics of the robot. A close-up of the signal in Fig. 11-(a), shown in Fig. 11-(b), allows us to identify the artificial equivalents of the variables that biologists have defined as relevant descriptors of earthworms' locomotion (stride length, protrusion time and stance time). The measured average values of these values are shown in Table II. Notice that further analysis of the experimental robot's kinematics can provide important information to increase the efficiency of the system. This is a matter of current and further research.

VI. CONCLUSION AND FUTURE WORK

We presented a novel multi-casting-based fabrication method to create a multi-material multi-actuator earthworm-inspired soft robot. The composing robot's actuators are manufactured using curable liquid Ecoflex® 00-50 silicone (Smooth-On), reinforced with structural fibers and o-rings. In this proposed design, structural reinforcement of the actuators defines the functionality and controllability of the robotic system as a whole, as the control algorithms are based on the pre-programmability of the actuators' motions. The basic motions of an earthworm's section are replicated with the use of two soft artificial circular muscles (radial actuators) and a soft artificial longitudinal muscle (axial actuator). By performing three experimental tests, the robot was demonstrated to locomote inside pipes, employing body motions inspired by earthworm burrowing. Notice that the modularity of the proposed design will allow for the future creation of longer structures, programable using other earthworm-inspired locomotion, such as peristalsis-based crawling.

In this work, we empirically explored the basic capabilities of burrowing-based locomotion inside pipes only. However, we anticipate that further research will produce modified and

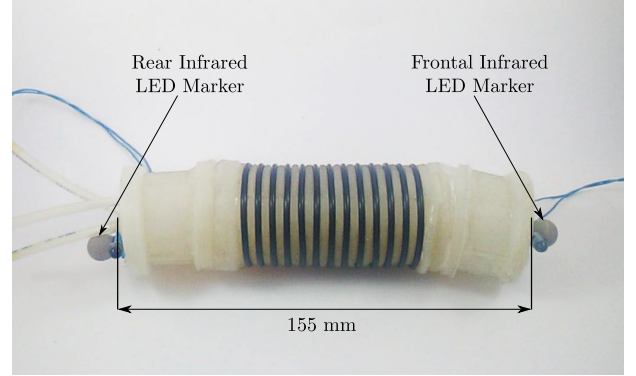


Fig. 10: **Twin prototype.** Second robot built and tested at the University of Chile to perform kinematic tests using an OptiTrack® system. In this case, two infrared markers are attached to both distal ends of the robot.

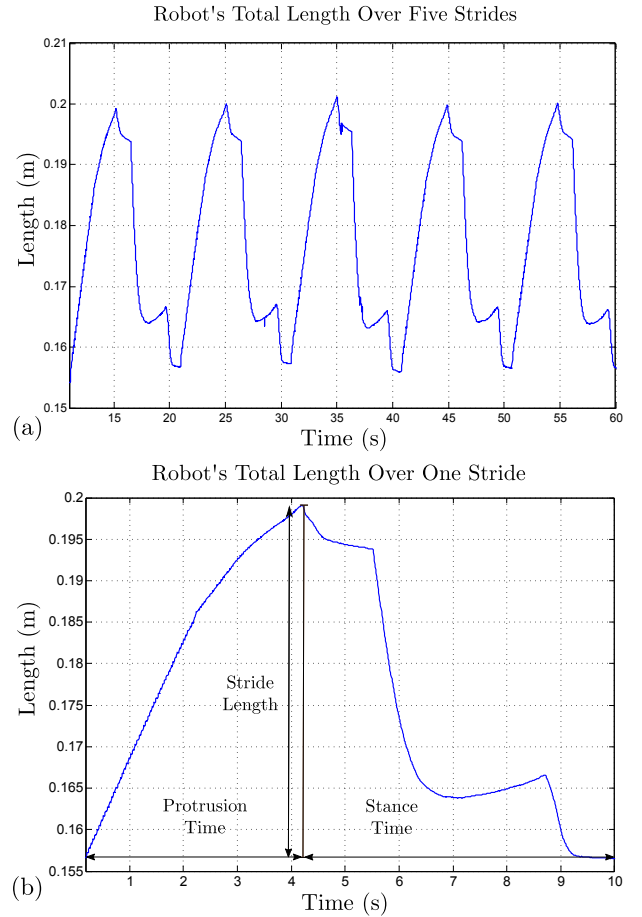


Fig. 11: **Kinematics of locomotion test.** Total length of the *twin* prototype while locomoting inside a 45°-inclined pipe. This signal was computed from the captured position of the two infrared markers shown in Fig. 10. (a) Total robot's length over five burrowing strides. (b) Total robot's length over one burrowing stride. The locomotion parameters *stride length*, *stance time* and *protrusion time* are indicated on the plot.

scaled-down versions of the proposed robotic concept and a great variety of applications. For example, in principle, it is possible to conceive the development of automated micro hollow-core catheters capable of navigating inside the human digestive and circulatory systems. A main potential

advantage of such microrobots would be the ability to reach locations inside human bodies without the exertion of external forces and manual human intervention, which are main sources of medical errors in surgeries [39]. Thus, the features of soft robots could in the near future significantly increase safety in human-machine interactions. These new possibilities bring new challenges as the development of new bio-compatible components, dissolvable materials and energy sources (based on electrolysis [40] or combustion [41], [42], for example) would be necessary in order to achieve high standards of safety and autonomy. Similarly, soft-robotic-based autonomous safe operation requires the invention and implementation of novel experimental methods for sensing, control and wireless communications.

REFERENCES

- [1] C. P. Hickman, L. S. Roberts, S. L. Keen, A. Larson, H. I'Anson, and D. J. Eisenhour, *Integrated Principles of Zoology, 14th Edition*. New York, NY: McGraw-Hill Higher Education, 2008.
- [2] D. Sadava, D. M. Hillis, H. C. Heller, and M. R. Berenbaum, *Life: The Science of Biology, 9th Edition*. Sunderland, MA: Sinauer Associates Inc., 2011.
- [3] J. B. Reece, L. A. Urry, M. L. Cain, S. A. Wasserman, P. V. Minorski, and R. B. Jackson, *Campbell Biology, 10th Edition*. Glenview, IL: Pearson, 2014.
- [4] K. J. Quillin, "Kinematic Scaling of Locomotion by Hydrostatic Animals: Ontogeny of Peristaltic Crawling by the Earthworm *lumbricus terrestris*," *J. Exp. Biol.*, vol. 202, no. 6, pp. 661–674, Mar. 1999.
- [5] S. Seok, C. D. Onal, K.-J. Cho, R. J. Wood, D. Rus, and S. Kim, "Meshworm: A Peristaltic Soft Robot With Antagonistic Nickel Titanium Coil Actuators," *IEEE/ASME Trans. Mechatron.*, vol. 18, no. 5, pp. 1485–1497, Oct. 2013.
- [6] T. Nakamura, T. Kato, T. Iwanaga, and Y. Muranaka, "Development of a Peristaltic Crawling Robot Based on Earthworm Locomotion," *J. Robot. Mechatron.*, vol. 18, no. 3, pp. 299–304, Jun. 2006.
- [7] M. Schulke, L. Hartmann, and C. Behn, "Worm-Like Locomotion Systems: Development of Drives and Selective Anisotropic Friction Structures," in *Proc. 56th Int. Scientific Colloq.*, Ilmenau, Germany, Sep. 2011.
- [8] T. Saito, T. Kagiwada, and H. Harada, "Development of an Earthworm Robot with a Shape Memory Alloy and Braided Tube," *Adv. Robot.*, vol. 23, no. 12–13, pp. 1743–1760, 2009.
- [9] B. Kim, M. G. Lee, Y. P. Lee, Y. Kim, and G. Lee, "An earthworm-like micro robot using shape memory alloy actuator," *Sensors Actuat. A: Phys.*, vol. 125, no. 2, pp. 429–437, Jan. 2006.
- [10] N. Saga and T. Nakamura, "Development of a peristaltic crawling robot using magnetic fluid on the basis of the locomotion mechanism of the earthworm," *Smart Mater. Struct.*, vol. 13, no. 3, pp. 566–569, May 2004.
- [11] J. Zuo, G. Yan, and Z. Gao, "A micro creeping robot for colonoscopy based on the earthworm," *J. Med. Eng. & Technol.*, vol. 29, no. 1, pp. 1–7, Jan. 2005.
- [12] K. Wang, G. Yan, G. Ma, and D. Ye, "An Earthworm-Like Robotic Endoscope System for Human Intestine: Design, Analysis, and Experiment," *Ann. Biomed. Eng.*, vol. 37, no. 1, pp. 210–221, Jun. 2009.
- [13] M. Kubota and T. Noritsugu, "Development of In-Pipe Mobile Robot Using Pneumatic Soft-Actuator," in *Proc. JFPS Int. Symp. Fluid Power*, 1999, pp. 195–200.
- [14] T. Noritsugu and M. Kubota, "Development of In-Pipe Mobile Robot using Pneumatic Soft-Actuator," *J. Robot. Soc. Japan*, vol. 18, no. 6, pp. 831–838, Aug. 2000.
- [15] R. F. Shepherd, F. Ilievski, W. Choi, S. A. Morin, A. A. Stokes, A. D. Mazzeo, X. Chen, M. Wang, and G. M. Whitesides, "Multigait soft robot," *Proc. Nat. Acad. Sci.*, vol. 108, no. 51, pp. 20400–20403, Dec. 2011.
- [16] C. Majidi, "Soft Robotics: A Perspective—Current Trends and Prospects for the Future," *Soft Robot.*, vol. 1, no. 1, pp. 5–11, Jul. 2013.
- [17] J. K. Paik, R. K. Kramer, and R. J. Wood, "Stretchable Circuits and Sensors for Robotic Origami," in *Proc. 2011 IEEE/RSJ Int. Conf. Intell. Robots and Syst. (IROS 2011)*, San Francisco, CA, Sep. 2011, pp. 414–420.
- [18] R. K. Kramer, C. Majidi, R. Sahai, and R. J. Wood, "Soft Curvature Sensors for Joint Angle Proprioception," in *Proc. 2011 IEEE/RSJ Int. Conf. on Intell. Robots Syst. (IROS 2011)*, San Francisco, CA, Sep. 2011, pp. 1919–1926.
- [19] J. y. Nagase, S. Wakimoto, T. Satoh, N. Saga, and K. Suzumori, "Design of a variable-stiffness robotic hand using pneumatic soft rubber actuators," *Smart Mater. Struct.*, vol. 20, no. 10, p. 105015 (9pp), Oct. 2011.
- [20] T. Ranzani, M. Cianchetti, G. Gerboni, I. De Falco, G. Petroni, and A. Menciassi, "A modular soft manipulator with variable stiffness," in *Proc. 3rd Joint Workshop New Technol. Comput./Robot Assisted Surgery*, Verona, Italy, Sep. 2013.
- [21] K. C. Galloway, P. Polygerinos, C. J. Walsh, and R. J. Wood, "Mechanically Programmable Bend Radius for Fiber-Reinforced Soft Actuators," in *Proc. 2013 16th Int. Conf. Adv. Robot. (ICAR 2013)*, Montevideo, Uruguay, Nov. 2013.
- [22] R. V. Martinez, J. L. Branch, C. R. Fish, L. Jin, R. F. Shepherd, R. M. D. Nunes, Z. Suo, and G. M. Whitesides, "Robotic Tentacles with Three-Dimensional Mobility Based on Flexible Elastomers," *Adv. Mater.*, vol. 25, no. 2, pp. 205–212, Jan. 2013.
- [23] S. C. Obiajulu, E. T. Roche, F. A. Pigula, and C. J. Walsh, "Soft Pneumatic Artificial Muscles with Low Threshold Pressures for a Cardiac Compression Device," in *Proc. ASME 2013 Int. Design Eng. Tech. Conf. & Comput. Inform. Eng. Conf. (IDETC/CIE 2013)*, Portland, OR, Aug. 2013.
- [24] C. Laschi, M. Cianchetti, B. Mazzolai, L. Margheri, M. Follador, and P. Dario, "Soft Robot Arm Inspired by the Octopus," *Adv. Robot.*, vol. 26, no. 7, pp. 709–727, 2012.
- [25] K. Suzumori, "Elastic materials producing compliant robots," *Robot. Auton. Syst.*, vol. 18, no. 1–2, pp. 135–140, Jul. 1996.
- [26] K. Suzumori, S. Endo, T. Kanda, N. Kato, and H. Suzuki, "A Bending Pneumatic Rubber Actuator Realizing Soft-bodied Manta Swimming Robot," in *Proc. 2007 IEEE Int. Conf. Robot. Autom. (ICRA 2007)*, Rome, Italy, Apr. 2007, pp. 4975–4980.
- [27] D. Qin, Y. Xia, and G. M. Whitesides, "Soft lithography for micro- and nanoscale patterning," *Nat. Protoc.*, vol. 5, no. 3, pp. 491–502, Feb. 2010.
- [28] J. Kwon, S. Park, J. Park, and B. Kim, "Evaluation of the critical stroke of an earthworm-like robot for capsule endoscopes," *Proc. IMechE, Part H: J. Eng. Med.*, vol. 221, no. 4, pp. 397–405, May 2007.
- [29] I. Asimov, *Fantastic Voyage*. New York, NY: Bantam Books, 1966.
- [30] B. Tribelhorn and Z. Dodds, "Evaluating the Roomba: A low-cost, ubiquitous platform for robotics research and education," in *Proc. 2007 IEEE Int. Conf. Robot. Autom. (ICRA 2007)*, Rome, Italy, Apr. 2007, pp. 1393–1399.
- [31] M. Raibert, K. Blankespoor, G. Nelson, R. Playter, and the Big-Dog Team, "BigDog, the Rough-Terrain Quadruped Robot," in *Proc. of the 17th IFAC World Congr.*, Seoul, Korea, Jul. 2008, pp. 10822–10825.
- [32] S. Seok, A. Wang, M. Y. (M) Chuah, D. Otten, J. Lang, and S. Kim, "Design Principles for Highly Efficient Quadrupeds and Implementation on the MIT Cheetah Robot," in *Proc. 2013 IEEE Int. Conf. Robot. Autom. (ICRA 2013)*, Karlsruhe, Germany, May 2013, pp. 3307–3312.
- [33] H.-W. Park and S. Kim, "Quadrupedal galloping control for a wide range of speed via vertical impulse scaling," *Bioinspir. & Biomim.*, vol. 10, no. 2, p. 025003 (20pp), Mar. 2015.
- [34] S. Hirose, *Biologically Inspired Robots: Snake-like Locomotors and Manipulators*. New York, NY: Oxford University Press, 1993.
- [35] S. Hirose and H. Yamada, "Snake-Like Robots," *IEEE Robot. Automat. Mag.*, vol. 16, no. 1, pp. 88–98, Mar. 2009.
- [36] C. D. Onal and D. Rus, "Autonomous undulatory serpentine locomotion utilizing body dynamics of a fluidic soft robot," *Bioinspir. Biomim.*, vol. 8, no. 2, p. 026003 (10pp), Jun. 2013.
- [37] N. O. Pérez-Arancibia, P.-E. J. Duhamel, K. Y. Ma, and R. J. Wood, "Model-Free Control of a Hovering Flapping-Wing Microrobot," *J. Intell. Robot. Syst.*, vol. 77, no. 1, pp. 95–111, Jan. 2015.
- [38] Y.-L. Park, B. Chen, N. O. Pérez-Arancibia, D. Young, L. Stirling, R. J. Wood, E. C. Goldfield, and R. Nagpal, "Design and control of a bio-inspired soft wearable robotic device for ankle-foot rehabilitation," *Bioinspir. Biomim.*, vol. 9, no. 1, p. 016007 (17pp), Mar. 2014.
- [39] P. Joice, G. B. Hanna, and A. Cuschieri, "Errors enacted during endoscopic surgery—a human reliability analysis," *Appl. Ergon.*, vol. 29, no. 6, pp. 409–414, Dec. 1998.
- [40] H. Gensler, R. Sheybani, P.-Y. Li, R. Lo, and E. Meng, "An Implantable MEMS Micropump System for Drug Delivery in Small Animals," *Biomed. Microdevices*, vol. 14, no. 3, pp. 483–496, Jun. 2012.
- [41] R. F. Shepherd, A. A. Stokes, J. Freaque, J. Barber, P. W. Snyder, A. D. Mazzeo, L. Cademartiri, S. A. Morin, and G. M. Whitesides, "Using Explosions to Power a Soft Robot," *Angew. Chem. Int. Ed.*, vol. 52, no. 10, pp. 2892–2896, Mar. 2013.
- [42] M. T. Tolley, R. F. Shepherd, M. Karpelson, N. W. Bartlett, K. C. Galloway, M. Wehner, R. Nunes, G. M. Whitesides, and R. J. Wood, "An Untethered Jumping Soft Robot," in *Proc. 2014 IEEE/RSJ Int. Conf. Intell. Robots Syst. (IROS 2014)*, Chicago, IL, Sep. 2014, pp. 561–566.